Preprints of the 21st IFAC World Congress (Virtual)
Berlin, Germany, July 12-17, 2020

LQR Control of Moisture Distribution in Microwave Drying Process Based on a Finite Element Model of Parabolic PDEs

Marzieh Hosseini * **Anna Kaasinen** * **Guido Link** **
Timo Lähivaara * **Marko Vauhkonen** *

* *Department of Applied Physics, University of Eastern Finland, Kuopio, Finland (e-mail: {marzieh.hosseini, anna.kaasinen, timo.lahivaara, marko.vauhkonen}@uef.fi).*
** *Institute for Pulsed Power and Microwave Technology, Karlsruhe Institute of Technology, Karlsruhe, Germany (e-mail: guido.link@kit.edu).*

Abstract: The microwave drying process is a widely used technology in the drying of porous dielectric materials. Designing a controller for moisture distribution in this process can improve product quality and reduce energy consumption and production time. In this paper, a model-based controller for moisture distribution in an industrial microwave drying process is developed. The moisture and temperature in this process are described by a pair of partial differential equations (PDEs) and have both temporal and spatial variations. In this view, using a semi-discrete finite element approximation, the coupled system of PDEs is transformed into a system of ordinary differential equations (ODEs). Based on the discretized ODEs, a linear quadratic regulator (LQR) controller is designed to determine the power levels of multiple microwave sources in this process to reach and maintain the desired moisture level. Numerical simulations are carried out in three different drying scenarios. The results show that the proposed controller achieves a very good performance in tracking the desired moisture level.

Keywords: Distributed Parameter Systems, Linear Quadratic Regulator (LQR) Control, Finite Element Method, Microwave Drying, Moisture Control

1. INTRODUCTION

Microwave drying technology is a widely used technique in the drying of dielectric materials because of its features such as volumetric heating and fast evaporation rate, Zhu et al. (2015); Li et al. (2010). In addition, multiple microwave sources in this process make the selective heating possible.

One of the main objectives in this process is to reach as uniform moisture distribution inside the material as possible. This can significantly affect the material quality after the drying process and prevent excessive heating and severe damages in industries. Reduction of energy consumption and processing time are other important goals in the microwave drying process, which can lead to a significant increase in the production rate. To achieve these goals, an advanced multiple-input multiple-output (MIMO) controller should be developed for this process.

Model-based controllers as one of the approaches in designing an advanced controller, require having a mathematical model of the process. Dynamics of the microwave drying process described by the moisture and temperature of the drying material depend on both position and time. This is a feature of most of the industrial processes which characterize them among a special class of dynamic systems so-called distributed parameter systems (DPS). The DPSs are typically modeled with partial differential equations (PDEs).

Depending on the location of actuators and sensors, control of the processes described by PDEs is generally divided into two categories: boundary control and domain control, Krstic and Smyshlyaev (2008). Most of the studies on this type of control are carried out for boundary control, Xu and Dubljevic (2017); Montaseri and Yazdanpanah (2012). However, control of the microwave drying process is classified as domain control because of the volumetric heating of microwave sources. There are not many studies on domain control since in most of the industrial processes the actuation is non-intrusive and taken into account through the boundary conditions.

Control of the microwave drying process is discussed in several studies. However, in very few of them, feedback control has been developed for this process, and in most of them, only process monitoring and manipulation of input microwave power without automatic control have been studied, Cuccurullo et al. (2012); Li et al. (2010). In Sun (2016), adaptive and intelligent temperature control has been proposed for the microwave heating process. Although both microwave heating and microwave drying use the microwave sources as sources of the input energy, they have different dynamics. Temperature control is also

studied in Sanchez et al. (2000); Alonso et al. (2000) for the microwave drying process.

Moisture control is not studied in the microwave drying process to the best of our knowledge. One reason is the requirement for information about the moisture distribution inside the drying material. This can be challenging since the moisture distribution can only be measured using process tomography sensors, and currently only sensors for point measurements are available. Although combing process tomography with a control system can result in significant improvements in many industrial processes, very few applications so far have used process tomography for feedback control, Ruuskanen et al. (2006); Sbarbaro and Vergara (2015).

In this paper, we develop an optimal controller based on the linear quadratic regulator (LQR) control to determine the power levels of multiple microwave sources. The objective is to reach as homogeneous moisture distribution as possible inside the porous material and the average moisture of the material should follow the desired moisture level. In this study, the porous material is a sample of wood, placed inside the microwave oven. We intend to use the electrical capacitance tomography (ECT) sensor in the microwave drying process to assist the controller with the moisture measurements. However, the integration of the ECT with the process control is not discussed in this paper. The temperature distribution on the surface of the material will also be available through an infrared camera.

To derive the process model as the requirement of designing the LQR controller, the Luikov model of heat and moisture transfer consisting of a pair of coupled parabolic PDEs is employed in this paper, Luikov (1975); Kocaefe et al. (2006). Additionally, the microwave power term is integrated with these PDEs. Using the semi-discrete finite element method (FEM), we discretize the model spatially, which results in a system of ODEs. These ODEs describe the moisture and temperature dynamics at each node of the discretization mesh. Therefore, the dimension of the system is very large and depends on the mesh density. The Maxwell equations are solved using the COMSOL Multiphysics to calculate the electric field from which the microwave power absorption can be obtained. Finally, an LQR controller is developed to derive the average of the states, describing the moisture distribution to the desired value by determining the power level of each microwave source.

This paper is structured as follows. In Section 2, the mathematical modeling of the microwave drying process using the finite element discretization is explained. In Section 3, an LQR controller is developed for the microwave drying process, and the simulation results are given in Section 4. Concluding remarks are given in Section 5.

2. MATHEMATICAL MODELLING

The microwave drying process is a very complicated process that involves the coupling of electromagnetic and simultaneous heat and moisture transfer through a porous sample. A schematic picture of this process is illustrated in Fig. 1. The porous dielectric material with high moisture content is placed inside the cavity while it is exposed to 6

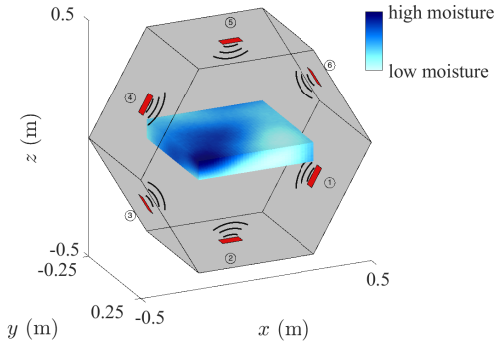

Fig. 1. A schematic picture of a microwave drying process.

microwave sources. The goal is to dry this material to reach the desired moisture level by adjusting the power levels of these microwave sources using a MIMO controller.

To design this controller, a mathematical model of the process is required to obtain quantitative information about the moisture and temperature distributions inside the material. In this study, a three-dimensional coupled pair of parabolic PDEs are used to formulate this problem. It is assumed that the sample is homogeneous, and the thermophysical properties are constant.

The moisture and heat transfer equations describing the behavior of the porous material during the drying process (modified from Luikov (1975); Kocaefe et al. (2006)) are:

$$\rho \frac{\partial}{\partial t}\left[\frac{M}{100}\right] = \nabla \cdot \left[\left(\frac{k_m \delta}{c_m}\right)\nabla T + \frac{k_m}{100 c_m}\nabla M\right] \quad (1)$$

and

$$\rho c_q \frac{\partial T}{\partial t} = \nabla \cdot \left[\left(k_q + \frac{\mu \lambda k_m \delta}{c_m}\right)\nabla T + \frac{\mu \lambda k_m}{100 c_m}\nabla M\right] + P_{mw}, \quad (2)$$

respectively. The PDEs (1-2) are defined in the domain $G =]-0.25, 0.25[\times]-0.25, 0.25[\times]-0.04, 0.04[$ with boundary ∂G and outward unit normal n. In (1-2), M is the dry-basis moisture content percentage, T is the temperature, k_m is the moisture conductivity, k_q is the thermal conductivity, c_m is the moisture capacity, c_q the heat capacity, δ is the thermal gradient coefficient, ρ is the density, λ is the latent heat of vaporization, and μ is the ratio of vapor diffusion coefficient to the coefficient of total moisture diffusion. In (2), P_{mw} is the power absorbed per unit volume in the material. The boundary conditions for the PDEs (1-2) are

$$\frac{-k_m}{100 c_m}\frac{\partial M}{\partial n} = \left(\frac{k_m \delta}{c_m}\right)\frac{\partial T}{\partial n} + \frac{h_m}{100 c_m}(M - M_g) \quad (3)$$

$$-k_q \frac{\partial T}{\partial n} = h_q (T - T_g) + \frac{(1-\mu)\lambda h_m}{100 c_m}(M - M_g), \quad (4)$$

where h_q is the convective heat transfer coefficient, h_m is the convective mass transfer coefficient, M_g is the ambient gas moisture content, and T_g is the ambient gas temperature. Also the initial conditions are defined as $M(0) = M_0$ and $T(0) = T_0$.

An approximation of the power absorption P_{mw} in (2) is needed. The absorbed power from m-th source is computed using the Poynting theorem as, Ayappa et al. (1991),

$$P_{mw}^{m}(x,y,z) = \frac{1}{2}\omega\epsilon_0\epsilon''||E^m(x,y,z)||^2, \tag{5}$$

where ω is the angular frequency, ϵ_0 is the vacuum permittivity, ϵ'' is the dielectric loss factor, and $E^m(x,y,z)$ is the electric field of the m-th source. Considering multiple microwave sources, calculating the microwave heating term is difficult because of complex microwave heating power superpositions. In this paper, it is assumed that the electric fields from different sources are incoherent. In this case, the superposed heating power is equivalent to the summation of heating powers of individual sources, Sun (2016).

There are 6 microwave sources with adjustable power levels in this testbed application. Therefore, the total effective microwave heating power can be written as

$$P_{mw}(x,y,z) = \sum_{m=1}^{6} P_{mw,\max}^{m}(x,y,z)u_m, \tag{6}$$

where $P_{mw,\max}^{m}(x,y,z)$ is the maximum heating power from the m-th source and $u_m \in [0,1]$ is the microwave source power level. Having (5) and (6), the heating power density in (2) can be written as

$$P_{mw}(x,y,z) = \frac{1}{2}\omega\epsilon_0\epsilon''\bar{E}u, \tag{7}$$

where $\bar{E} = \left[||E_{\max}^{1}(x,y,z)||^2,\ldots,||E_{\max}^{6}(x,y,z)||^2\right] \in \mathbb{R}^{1\times 6}$ is a vector in which each element represents the computed maximum electric field intensity for each microwave source and $u = [u_1,\ldots,u_6]^T$. In this study, the electric field is calculated using the COMSOL Multiphysics.

The electric field is correlated with the loss factor and hence the moisture. Therefore, as the moisture content of the material and the loss factor change, the electric field should be recalculated. However, we have assumed that both the electric field and the loss factor remain constant throughout the drying process to simplify the model.

To compute the finite element approximation of PDEs (1-2), the variational form is needed which is derived as follows. Let $V = H^1(G) = \{v : ||v|| + ||\nabla v|| < \infty\}$, multiplying (1) with a test function $v_1 \in V$ gives

$$\frac{\rho}{100}\left\langle\frac{\partial M}{\partial t}, v_1\right\rangle_0 = \left\langle\nabla\cdot\left(\frac{k_m\delta}{c_m}\nabla T + \frac{k_m}{100c_m}\nabla M\right), v_1\right\rangle_0, \tag{8}$$

where $\langle\cdot,\cdot\rangle_0$ is the inner product in the Lebesgue space $L_2(G)$. Using the Green's formula for integration by parts and denoting the surface measure on ∂G by $d\sigma$ we have

$$\begin{aligned}\frac{\rho}{100}\left\langle\frac{\partial M}{\partial t}, v_1\right\rangle_0 =& -\frac{k_m\delta}{c_m}\left[\langle\nabla T,\nabla v_1\rangle_0 - \int_{\partial G}\frac{\partial T}{\partial n}v_1\,d\sigma\right]\\ &- \frac{k_m}{100c_m}\left[\langle\nabla M,\nabla v_1\rangle_0 - \int_{\partial G}\frac{\partial M}{\partial n}v_1\,d\sigma\right].\end{aligned} \tag{9}$$

Applying the boundary conditions (3-4) in (9) results in

$$\begin{aligned}\frac{\rho}{100}\left\langle\frac{\partial M}{\partial t}, v_1\right\rangle_0 =& -\frac{k_m\delta}{c_m}\langle\nabla T,\nabla v_1\rangle_0\\ &- \frac{k_m}{100c_m}\langle\nabla M,\nabla v_1\rangle_0\\ &- \frac{h_m}{100c_m}\int_{\partial G}(M-M_g)\,v_1\,d\sigma.\end{aligned} \tag{10}$$

Similarly, multiplying (2) by another test function $v_2 \in V$ and using the Green's formula gives

$$\begin{aligned}\rho c_q\left\langle\frac{\partial T}{\partial t}, v_2\right\rangle_0 =& -\left(k_q + \frac{\mu\lambda k_m\delta}{c_m}\right)\langle\nabla T,\nabla v_2\rangle_0\\ &+ \left(k_q + \frac{\mu\lambda k_m\delta}{c_m}\right)\int_{\partial G}\frac{\partial T}{\partial n}v_2\,d\sigma\\ &- \frac{\mu\lambda k_m}{100c_m}\left[\langle\nabla M,\nabla v_2\rangle_0 - \int_{\partial G}\frac{\partial M}{\partial n}v_2\,d\sigma\right]\\ &+ \frac{1}{2}\omega\epsilon_0\epsilon''\left\langle\bar{E}u, v_2\right\rangle_0.\end{aligned} \tag{11}$$

Applying the boundary conditions (3-4) in (11) results in

$$\begin{aligned}\rho c_q\left\langle\frac{\partial T}{\partial t}, v_2\right\rangle_0 =& -\left(k_q + \frac{\mu\lambda k_m\delta}{c_m}\right)\langle\nabla T,\nabla v_2\rangle_0\\ &- \frac{\mu\lambda k_m}{100c_m}\langle\nabla M,\nabla v_2\rangle_0\\ &- h_q\int_{\partial G}(T-T_g)\,v_2\,d\sigma\\ &- \frac{\lambda h_m}{100c_m}\int_{\partial G}(M-M_g)\,v_2\,d\sigma\\ &+ \frac{1}{2}\omega\epsilon_0\epsilon''\left\langle\bar{E}u, v_2\right\rangle_0.\end{aligned} \tag{12}$$

Assuming the constant ambient gas moisture and temperature, we can define $\tilde{M} = M - M_g$ and $\tilde{T} = T - T_g$. Also the following vector notations are defined

$$\xi = \begin{bmatrix}\tilde{M}\\ \tilde{T}\end{bmatrix} \quad\text{and}\quad v = \begin{bmatrix}v_1\\ v_2\end{bmatrix}. \tag{13}$$

Adding (10) to (12), the variational form can be written as

$$\left\langle\begin{bmatrix}\frac{\rho}{100} & 0\\ 0 & \rho c_q\end{bmatrix}\frac{\partial\xi}{\partial t}, v\right\rangle_{L_2(G)\times L_2(G)} = a(\xi,v) + f(t,v), \tag{14}$$

where $\langle\boldsymbol{f},\boldsymbol{g}\rangle_{L_2(G)\times L_2(G)}$ for the vectors $\boldsymbol{f} = [f_1,f_2]^T$ and $\boldsymbol{g} = [g_1,g_2]^T$ is defined as

$$\langle\boldsymbol{f},\boldsymbol{g}\rangle_{L_2(G)\times L_2(G)} = \langle f_1,g_1\rangle_0 + \langle f_2,g_2\rangle_0. \tag{15}$$

The bilinear form $a(\xi,v)$ in (14) is

$$\begin{aligned}a(\xi,v) =& a_1\left\langle\nabla\tilde{T},\nabla v_1\right\rangle_0 + a_2\left\langle\nabla\tilde{M},\nabla v_1\right\rangle_0\\ &+ a_3\left\langle\nabla\tilde{T},\nabla v_2\right\rangle_0 + a_4\left\langle\nabla\tilde{M},\nabla v_2\right\rangle_0\\ &- h_q\int_{\partial G}\tilde{T}v_2\,d\sigma + a_5\int_{\partial G}\tilde{M}v_2\,d\sigma\\ &+ a_6\int_{\partial G}\tilde{M}v_1\,d\sigma\end{aligned} \tag{16}$$

and

$$f(t,v) = \frac{1}{2}\omega\epsilon_0\epsilon''\left\langle\bar{E}u, v_2\right\rangle_0. \tag{17}$$

The coefficients a_i in (16) are $a_1 = -\frac{k_m\delta}{c_m}$, $a_2 = -\frac{k_m}{100c_m}$, $a_3 = -\left(k_q + \frac{\mu\lambda k_m\delta}{c_m}\right)$, $a_4 = -\frac{\mu\lambda k_m}{100c_m}$, $a_5 = -\frac{\lambda h_m}{100c_m}$, and $a_6 = -\frac{h_m}{100c_m}$.

Having the variational form (14), we can compute the finite element approximation. First, the solution domain G is discretized into small elements (tetrahedra in our case). Fig. 2 shows the mesh that is used for the finite element approximation consisting of 6993 elements and

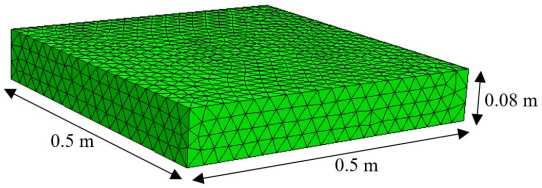

Fig. 2. The finite element mesh used in the calculations (with 1835 nodes and 6993 elements).

1835 nodes. Let $V_h \subset V$ be a finite-dimensional subspace, and $[\phi_1, \ldots, \phi_N]$ be the piece-wise linear basis functions for V_h. In FEM computations, the unknown variable ξ within the sample is approximated with the sum

$$\xi_h(x, y, z, t) = \sum_{j=1}^{2N} \alpha_j(t)\psi_j(x, y, z), \tag{18}$$

where N is the number of nodes in the discretized domain and

$$\{\psi_j\}_{j=1}^{2N} = \left\{ \begin{bmatrix} \phi_1 \\ 0 \end{bmatrix}, \cdots, \begin{bmatrix} \phi_N \\ 0 \end{bmatrix}, \begin{bmatrix} 0 \\ \phi_1 \end{bmatrix}, \cdots, \begin{bmatrix} 0 \\ \phi_N \end{bmatrix} \right\}. \tag{19}$$

Using the finite element approximation (18) in the variational form (14) results in

$$\left\langle \begin{bmatrix} \frac{\rho}{100} & 0 \\ 0 & \rho c_q \end{bmatrix} \frac{\partial \xi_h}{\partial t}, \psi_i \right\rangle_{L_2(G)\times L_2(G)} = a(\xi_h, \psi_i) + f(t, \psi_i) \tag{20}$$

for $i = 1, \cdots, 2N$. This can be written as

$$\mathbb{L}\dot{\alpha}(t) = \mathbb{K}\alpha(t) + Fu(t), \tag{21}$$

where

$$\mathbb{L} = \begin{bmatrix} \frac{\rho}{100}L & 0 \\ 0 & \rho c_q L \end{bmatrix} \tag{22}$$

with

$$L(i, j) = \langle \phi_j, \phi_i \rangle_0, \quad i, j = 1, \cdots, N \tag{23}$$

and $\mathbb{K}$ has a block structure as

$$\mathbb{K} = \begin{bmatrix} a_2K_d + a_6K_b & a_1K_d \\ a_4K_d + a_5K_b & a_3K_d - h_qK_b \end{bmatrix}, \tag{24}$$

where

$$K_d(i, j) = \langle \nabla\phi_j, \nabla\phi_i \rangle_0, \quad i, j = 1, \ldots, N \tag{25}$$

$$K_b(i, j) = \int_{\partial G} \phi_j\phi_i \, d\sigma, \quad i, j = 1, \ldots, N. \tag{26}$$

Also, the matrix F in (21) is of the form

$$F = \frac{1}{2}\omega\epsilon_0\epsilon'' \begin{bmatrix} 0_{N\times 6} \\ \langle \bar{E}, \phi_1 \rangle_0 \\ \vdots \\ \langle \bar{E}, \phi_N \rangle_0 \end{bmatrix}. \tag{27}$$

Equation (21) is a system of ODEs. Since the nature of the measurements is in discrete time, these equations are also discretized for time using the implicit Euler method as

$$X(k+1) = \left(I - \Delta t\mathbb{L}^{-1}\mathbb{K}\right)^{-1} \left[X(k) + \Delta t\mathbb{L}^{-1}Fu(k)\right], \tag{28}$$

where $X(k) = [\alpha_1(t_k), \alpha_1(t_k), \cdots, \alpha_{2N}(t_k)]^T$ and Δt is the sample time. Having (28), the discrete-time state space form of the process model can be obtained by

$$X(k+1) = A_dX(k) + B_du(k), \tag{29}$$

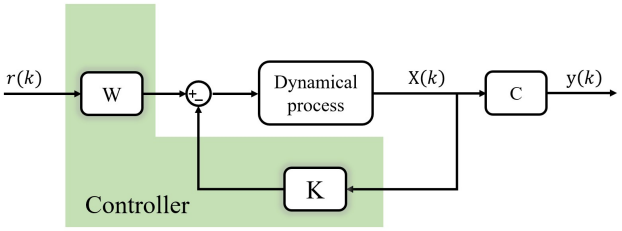

Fig. 3. The designed LQR controller structure.

where $X \in \mathbb{R}^{2N}$ is the state vector of the system, $u \in \mathbb{R}^6$ is the vector of power levels of the microwave sources as the control input, and

$$A_d = \left(I - \Delta t\mathbb{L}^{-1}\mathbb{K}\right)^{-1} \tag{30}$$

$$B_d = A_d\Delta t\mathbb{L}^{-1}F. \tag{31}$$

3. MOISTURE CONTROL

The state vector in (29) has $2N$ elements. The first N elements describe the moisture content at each node in the domain G, and the next N elements describe the temperature value of each node. The dimension of the state vector depends on the discretization mesh density. In this paper, we are using a mesh with 1835 nodes, so the dimension of the state vector is 3670, while only 6 control inputs are available. As can be shown, these types of systems are not controllable and observable within the classical definitions.

The control objective in the microwave drying process is to reach as homogeneous moisture distribution as possible such that it satisfies a desired average value. With only 6 control inputs and 3670 states, it is neither possible nor necessary to control the moisture and temperature of each node. We have selected several control methods to design the controller for this process and as the first method, the controller in this paper is developed using the LQR control method. In this approach, the average moisture of the whole material is taken as the system output and the goal is to have this value converged to the desired moisture level. We assume that the moisture and temperature value at each node is available. This is not far from the practical case since the ECT sensor can provide us with the moisture distribution instead of conventional point measurements. However, the temperature is measured only at the top surface of the material, but having a thin material we can assume that the temperature in the depth is the same as on the surface. The controller is designed based on the classical LQR control with the set-point tracking scheme. The controller structure is shown in Fig. 3.

In the LQR control, the goal is to solve the minimization problem

$$\min_u \sum_{k=0}^{\infty} X^T(k)QX(k) + u^T(k)Ru(k),$$
$$\text{s.t.} \quad X(k+1) = A_dX(k) + B_du(k), \tag{32}$$

where $Q \geq 0$ and $R > 0$ are the weight matrices which affect the state convergence speed and the control effort magnitude. Since the objective is to control the moisture content without the temperature control, the matrix Q is chosen as

$$Q = 10 \begin{bmatrix} I_N & 0 \\ 0 & 0 \end{bmatrix} \tag{33}$$

and the matrix $R = 1000 I_6$. The minimization of (32) results in the controller gain

$$K = \left(R + B_d^T S B_d\right)^{-1} B_d^T S A_d, \tag{34}$$

where S is obtained by solving the algebraic Riccati equation

$$S = A_d^T S A_d - A_d^T S B_d \left(R + B_d^T S B_d\right)^{-1} B_d^T S A_d + Q. \tag{35}$$

The final control law is determined by

$$u(k) = -KX(k) + Wr(k), \tag{36}$$

where $r(k)$ is the desired moisture level. The first term in (36) stabilizes the closed-loop system such that the closed-loop matrix $(A_d - B_d K)$ is Hurwitz. The second term in (36) is embedded in the control law to eliminate the steady-state error and track the desired moisture.

Having the state space equation (29) and the control law (36), the closed loop equations for the whole system are

$$X(k+1) = (A_d - B_d K) X(k) + B_d W r(k) \tag{37}$$

$$y(k) = CX(k). \tag{38}$$

To have $y(k) \to r(k)$, the DC-gain from r to y should be unit, that is

$$C \left(I - (A_d - B_d K)\right)^{-1} B_d W = I. \tag{39}$$

Taking the average moisture value as the system output results in $C = \frac{1}{N} [\mathbf{1}_{1\times N}\ 0_{1\times N}]$. Using this C in (39), the $W \in \mathbf{R}^{6\times 1}$ can be computed using the least square method.

4. RESULTS AND DISCUSSION

In this section, the results of numerical simulations are presented to study the performance of the proposed model and controller. The material parameters are taken from Kocaefe et al. (2006). The ambient temperature and moisture are chosen as $T_g = 373$ K and $M_g = 5\%$, respectively, and the initial temperature $T_0 = 298$ K.

In the first scenario, it is assumed that the material has homogeneous initial moisture and temperature distributions. The initial moisture is 80%, and the desired moisture level is 15%. Fig. 4 shows the average moisture of the material during the drying process with the LQR controller. As seen, the moisture decreases faster at the beginning of the drying because of the large difference between the initial moisture and the ambient gas moisture, which results in a large gradient between the boundaries and the ambient gas. As it reaches the desired moisture level, it stops decreasing and stays at the same value. In this scenario, the steady-state error of the average moisture is 0.4% which is small enough. The control actions corresponding to this simulation are presented in Fig. 5. The control inputs are the power levels of the microwave sources, which can vary continuously between 0 and 1. The input 0 means no microwave power, and 1 is for the case of maximum power, which is 2 kW per microwave source in our application. The output control command from the LQR controller is saturated to satisfy this practical constraint. Before reaching the desired moisture, all microwave sources are working at their maximum level, and after that, the control inputs converge to 0. To monitor the moisture distribution of the

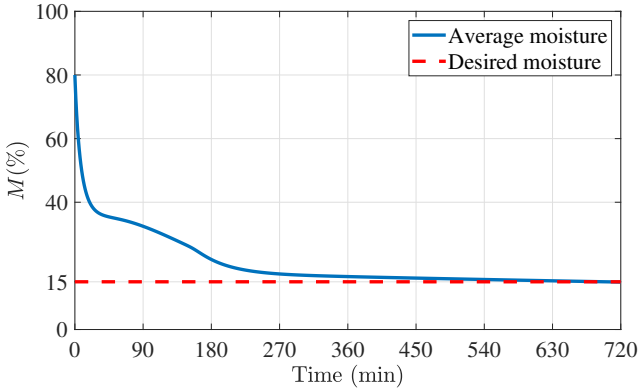

Fig. 4. The average moisture content of the material during the drying process with the LQR controller in the homogeneous case.

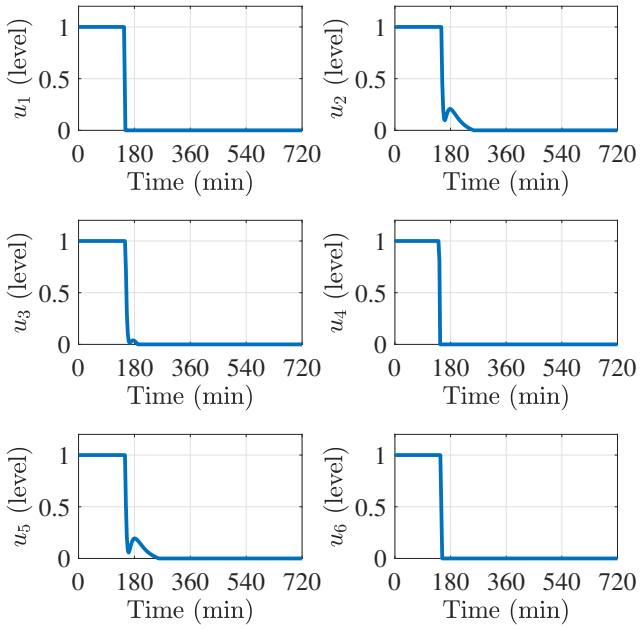

Fig. 5. The control inputs with the LQR controller during the drying process in the homogeneous case.

material during the drying process, Fig. 6 illustrates this distribution at different time instants. As mentioned, the objective of this process is to reach as homogeneous moisture distribution as possible. It is clear that the moisture profiles are symmetric and the moisture reduces gradually with time. Also, it can be seen that the moisture removal near the boundaries is faster than inside the domain, as expected.

In the second scenario, a case with non-homogeneous initial moisture distribution is studied. In this case, it is assumed that one half of the material has 50%, and the other half has 80% moisture content as the initial value. Fig. 7 shows the initial moisture distribution in this simulation. As in the previous scenario, the desired moisture value for the whole material is 15%. The average moisture of the material during the drying process with the LQR control, in this case, is shown in Fig. 8. As seen, the average moisture converges to the desired value despite having a non-homogeneous initial condition. The steady-state error of the average moisture in this scenario is 2.6%.

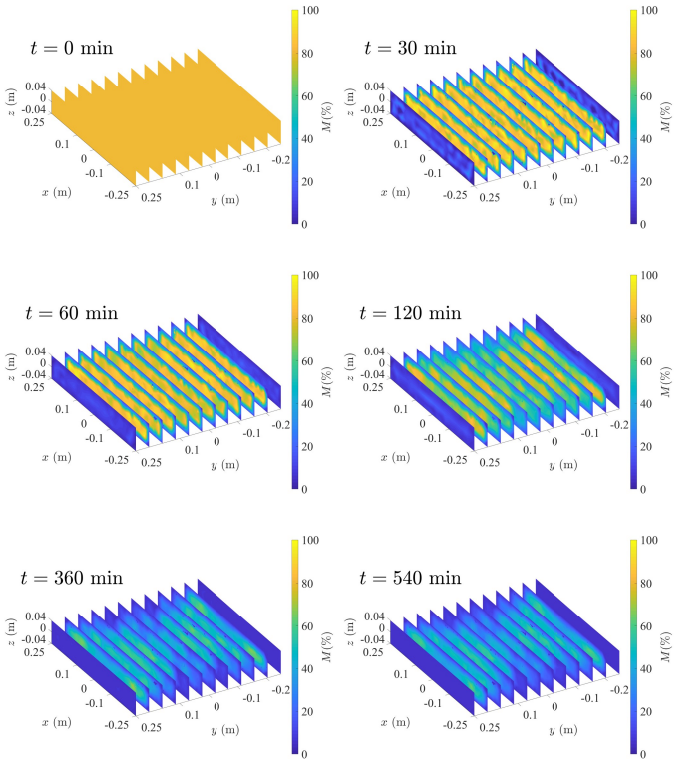

Fig. 6. The moisture distribution of the material during the drying process with the LQR controller in the homogeneous case.

Comparing these two scenarios, we can see that in the non-homogeneous case, the initial moisture content on the right half of the material is the same as in the homogeneous case (80%). However, the initial moisture on the left side is lower than the initial moisture of the homogeneous case. Having this information, the control inputs in these two cases can be studied. According to Fig. 1, the left side of the material is located on the same side as the sources 3 and 4. Since the initial moisture content on this side is lower in the second scenario, lower power levels for these two sources are expected. Fig. 9 shows the control inputs in these two scenarios. As seen, the control inputs for the microwave sources 3 and 4 decreases earlier in the non-homogeneous case, as expected. The microwave sources 2 and 5 are located between two sides, and since the overall initial moisture is lower in the non-homogeneous case, the control inputs for these two sources also decrease earlier in the second scenario. However, this decrease is not as large as the decrease of control inputs for sources 3 and 4, which is expected.

In the last scenario, we studied a case in which the drying process starts with an 80% homogeneous moisture, and the desired moisture level is 20% at the beginning of the simulation. However, after some time, the desired moisture level changes, and is decreased to 10%. The average moisture of the material with the LQR controller in this simulation is demonstrated in Fig. 10. It can be seen that it converges to 20% at first, and after the step change in the desired moisture, the average moisture decreases to the new desired level, which is 10%. The steady-state error of the average moisture is 2% for the first desired moisture,

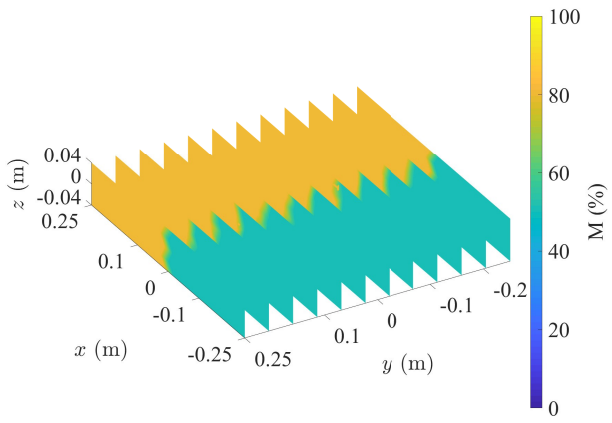

Fig. 7. The initial moisture distribution of the material in the non-homogeneous case.

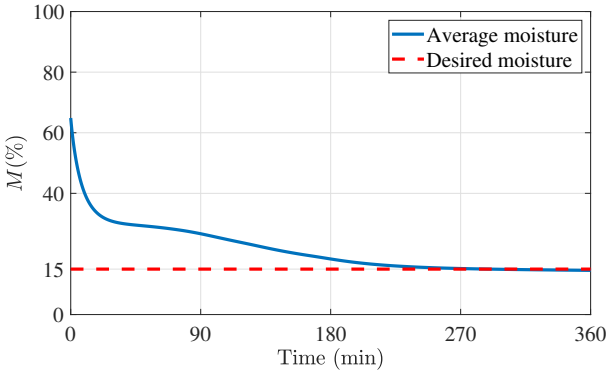

Fig. 8. The average moisture content of the material during the drying process with the LQR controller in the non-homogeneous case.

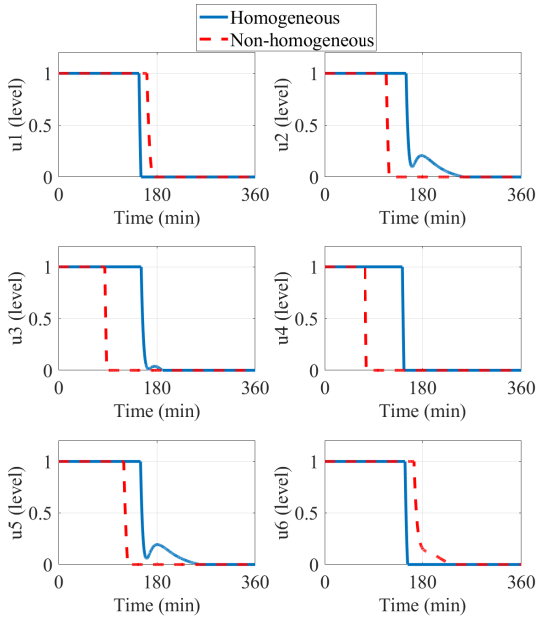

Fig. 9. The comparison between the control inputs with the LQR controller in the homogeneous and non-homogeneous cases.

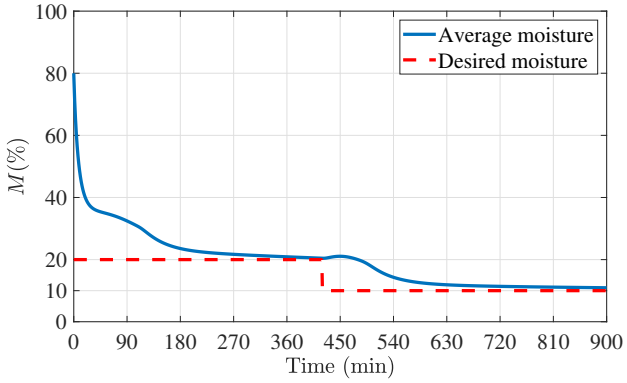

Fig. 10. The average moisture content of the material during the drying process with the LQR controller in the case of a step change in the desired moisture.

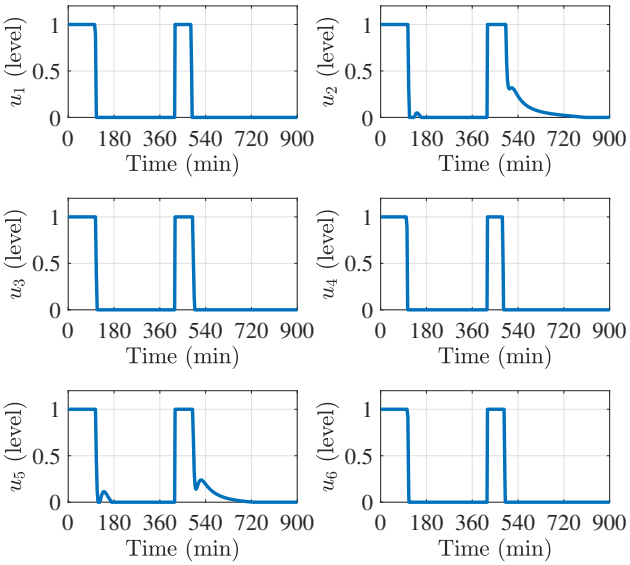

Fig. 11. The control inputs with the LQR controller during the drying process in the case of a step change in the desired moisture.

and 9% for the second one. As shown, the average moisture takes more time to converge to a lower desired moisture. The corresponding control inputs are also shown in Fig. 11. It can be seen that the microwave power increases after the step change to satisfy the new desired moisture level.

5. CONCLUSIONS

In this paper, we used the FEM to semi-discretize a model for the microwave drying process, which was based on a coupled system of PDEs. The derived model was used to calculate both moisture and temperature distributions inside the material. The LQR controller was then developed based on the discretized model. Numerical simulations demonstrated an impressive performance of this controller in tracking the desired moisture level, both with homogeneous and non-homogeneous initial moisture distributions. A simulation case of a time-varying desired moisture also produced very good results.

ACKNOWLEDGEMENTS

This work has been supported by the European Union's Horizon 2020 Research and Innovation Programme under the Marie Skłodowska-Curie grant agreement No 764902 (TOMOCON-www.tomocon.eu), and by the Academy of Finland (Finnish Centre of Excellence of Inverse Modelling and Imaging, project number 312344, and project number 321761).

REFERENCES

Alonso, A.A., Banga, J.R., and Sanchez, I. (2000). Passive control design for distributed process systems: Theory and applications. *AIChE Journal*, 46(8), 1593–1606.

Ayappa, K., Davis, H., Crapiste, G., Davis, E., and Gordon, J. (1991). Microwave heating: an evaluation of power formulations. *Chemical Engineering Science*, 46(4), 1005 – 1016.

Cuccurullo, G., Giordano, L., Albanese, D., Cinquanta, L., and Di Matteo, M. (2012). Infrared thermography assisted control for apples microwave drying. *Journal of Food Engineering*, 112(4), 319–325.

Kocaefe, D., Younsi, R., Chaudry, B., and Kocaefe, Y. (2006). Modeling of heat and mass transfer during high temperature treatment of aspen. *Wood Science and Technology*, 40(5), 371–391.

Krstic, M. and Smyshlyaev, A. (2008). *Boundary control of PDEs: A course on backstepping designs*, volume 16. Siam.

Li, Z., Raghavan, G., and Orsat, V. (2010). Temperature and power control in microwave drying. *Journal of Food Engineering*, 97(4), 478–483.

Luikov, A.V. (1975). Systems of differential equations of heat and mass transfer in capillary-porous bodies. *International Journal of Heat and Mass Transfer*, 18(1), 1–14.

Montaseri, G. and Yazdanpanah, M.J. (2012). Predictive control of uncertain nonlinear parabolic PDE systems using a Galerkin/neural-network-based model. *Communications in Nonlinear Science and Numerical Simulation*, 17(1), 388–404.

Ruuskanen, A., Seppänen, A., Duncan, S., Somersalo, E., and Kaipio, J. (2006). Using process tomography as a sensor for optimal control. *Applied Numerical Mathematics*, 56(1), 37–54.

Sanchez, I., Banga, J.R., and Alonso, A.A. (2000). Temperature control in microwave combination ovens. *Journal of Food Engineering*, 46(1), 21–29.

Sbarbaro, D. and Vergara, S. (2015). Design of a control system based on EIT sensors: An optimization based approach. *IFAC-PapersOnLine*, 48(25), 218–222.

Sun, Y. (2016). *Adaptive and Intelligent Temperature Control of Microwave Heating Systems with Multiple Sources*. Ph.D. thesis, KIT Scientific Publishing, Karlsruhe.

Xu, X. and Dubljevic, S. (2017). Output regulation for a class of linear boundary controlled first-order hyperbolic PIDE systems. *Automatica*, 85, 43–52.

Zhu, H., Gulati, T., Datta, A.K., and Huang, K. (2015). Microwave drying of spheres: Coupled electromagnetics-multiphase transport modeling with experimentation. part I: Model development and experimental methodology. *Food and Bioproducts Processing*, 96, 314–325.